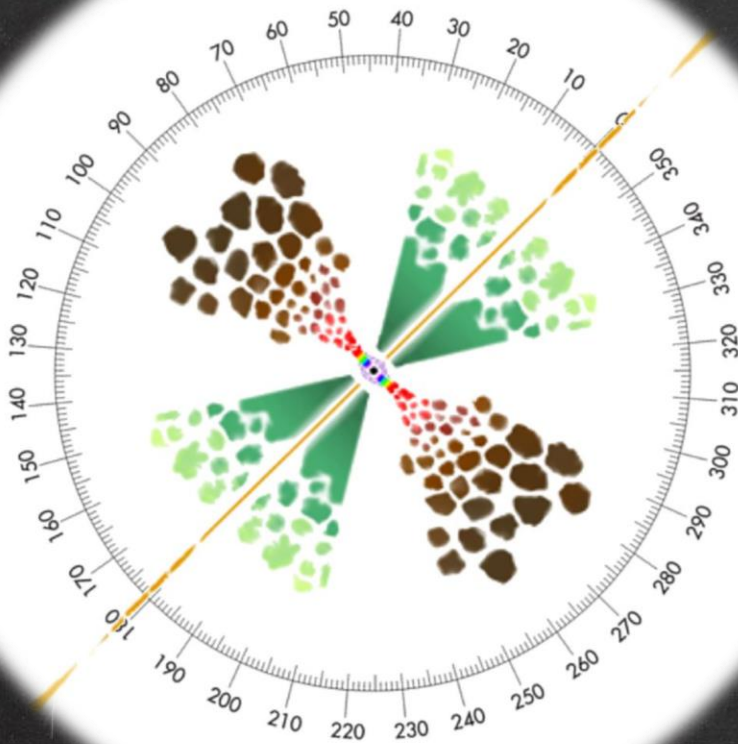


Marin 2016



Ionized gas in AGN is present on all scales, from few r_g to several kpc

Despite the complex phenomenology, the physics of this gas is governed by a few fundamental principles.

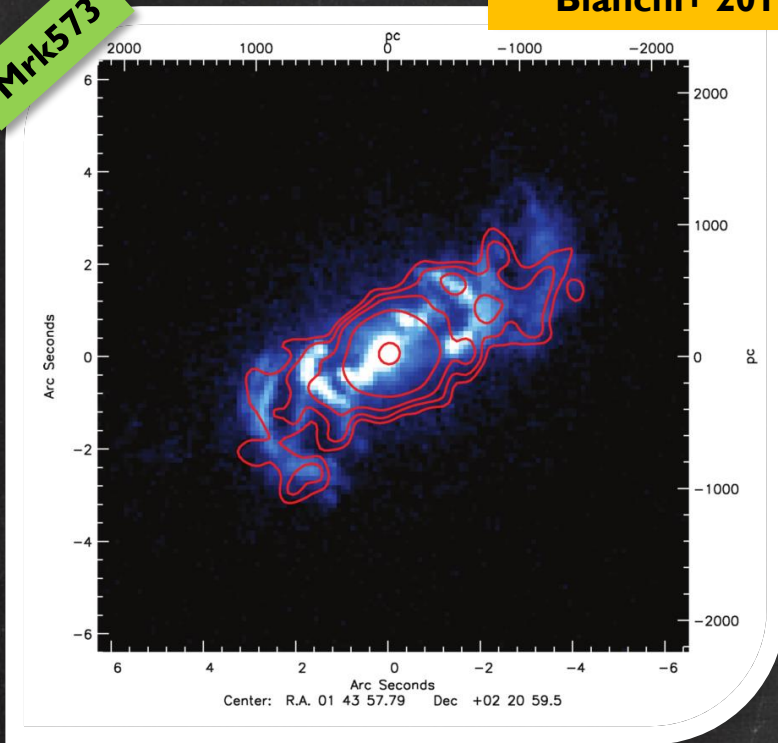
The nuclear strong radiation field is likely the only ionization and heating source

Gas dynamics in some regions is almost completely governed by the Black Hole mass

The consequences of these first principles lead to clear predictions that can be tested experimentally

Mrk573

Bianchi+ 2010



The coincidence between the soft X-ray and [O III] emission is striking in most sources observed by *Chandra* and *HST*, both in extension and in morphology (e.g. Bianchi+, 2006)

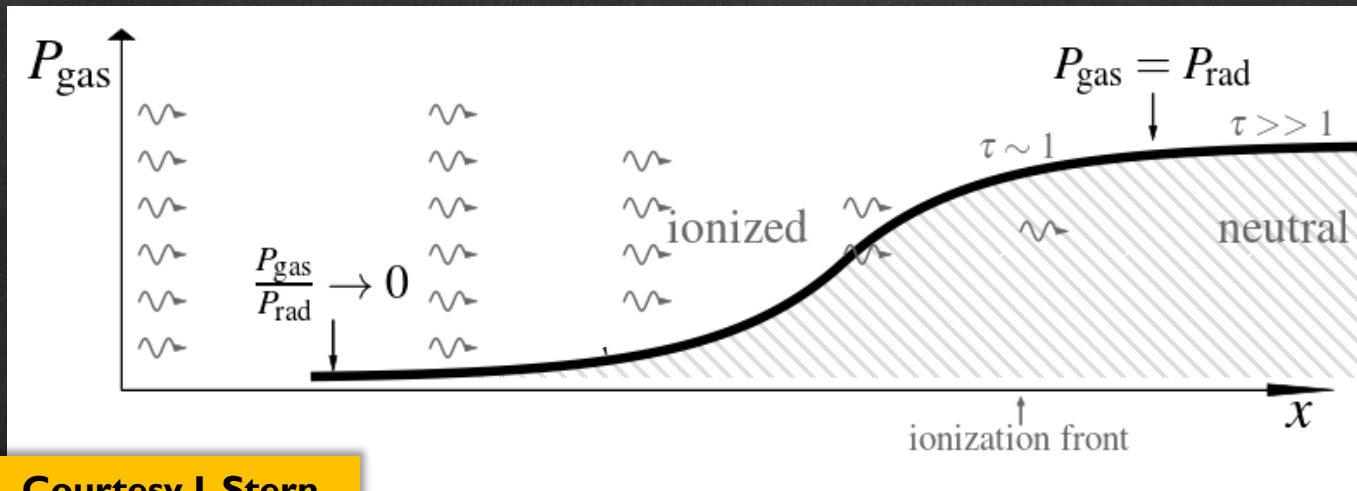
The same gas, photoionized by the AGN continuum, and extended on $\sim 100s$ pc, produces both the soft X-ray emission lines and the NLR optical emission

- Inconsistent with a single- U model \rightarrow requires high- U and low- U phases
 - The [O III]/soft X-ray ratio is spatially constant $\rightarrow n \propto r^{-2}$
 - The [O III]/soft X-ray ratio is fairly universal among the sources



Radiation Pressure Compression

Mathews 67; Pier&Voit 95; Dopita+02;
Rózańska+06; Pellegrini+07,09; Draine 11;
Yeh&Matzner 12; Stern+14a,b; Baskin+14a,b



Courtesy J. Stern

ASSUMPTIONS

- ✓ Radiation is the dominant force acting on the gas
- ✓ The ambient pressure is much lower than radiation pressure

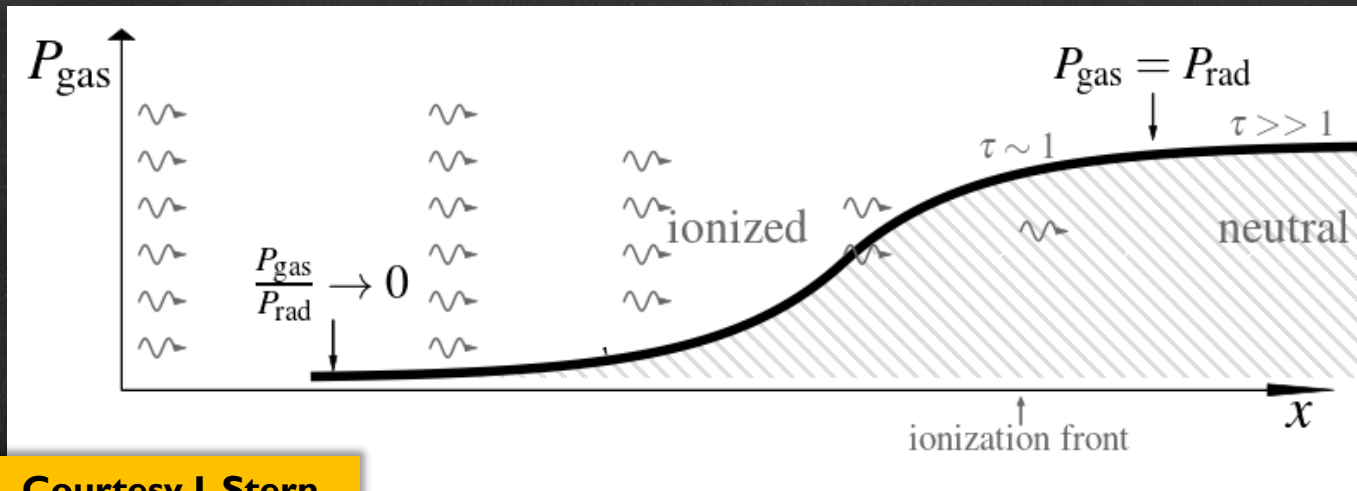
CONSEQUENCES

The radiation is absorbed in the surface layer of the gas, both ionizing it and compressing it, thus increasing its pressure

The pressure of the incident radiation itself can confine the ionized layer of the illuminated gas: **the gas is Radiation Pressure Compressed**

Radiation Pressure Compression

Mathews 67; Pier&Voit 95; Dopita+02;
Rózańska+06; Pellegrini+07,09; Draine 11;
Yeh&Matzner 12; Stern+14a,b; Baskin+14a,b



Courtesy J. Stern

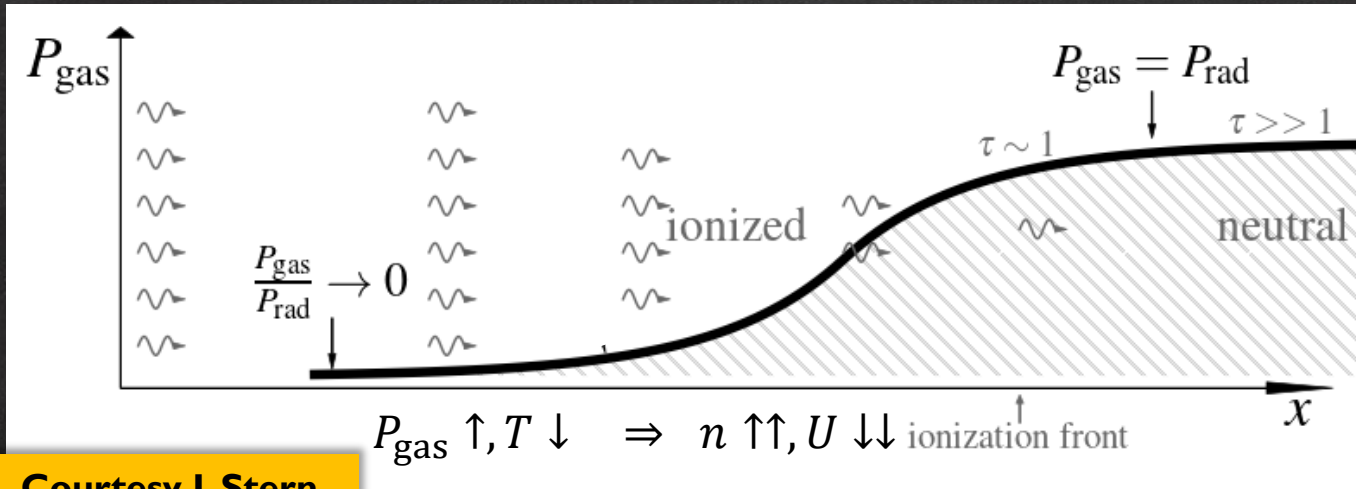
At $\tau \gg 1$, all the radiation is absorbed, and there is a transition to neutral gas

At $\tau \sim 1$, the gas pressure roughly equals the radiation pressure: this layer is called the **ionization front**

Near the ionization front, at the boundary between the H II and H I layers, the temperature is always $T_f \sim 10^4 \text{ K}$, and the equality of gas pressure and radiation pressure implies that the ionization parameter is always ~ 0.03

Radiation Pressure Compression

Mathews 67; Pier&Voit 95; Dopita+02;
 Rózańska+06; Pellegrini+07,09; Draine 11;
 Yeh&Matzner 12; Stern+14a,b; Baskin+14a,b



Courtesy J. Stern



- ✓ **A large range of n and U in a single slab:** the same gas which emits the low-ionization emission lines has a highly ionized surface which emits X-ray lines
- ✓ At the ionization front, the temperature is universal and $P_{\text{gas}} = P_{\text{rad}}$: since the latter is $\propto r^{-2}$, then $n \propto r^{-2}$
- ✓ The hydrostatic solution of RPC gas is independent of the boundary values at the illuminated surface $(U_0, n_0, P_{\text{gas},0})$: **RPC models are universal and have essentially zero free parameters**

SOFT X-RAY EMISSION IN OBSCURED AGN

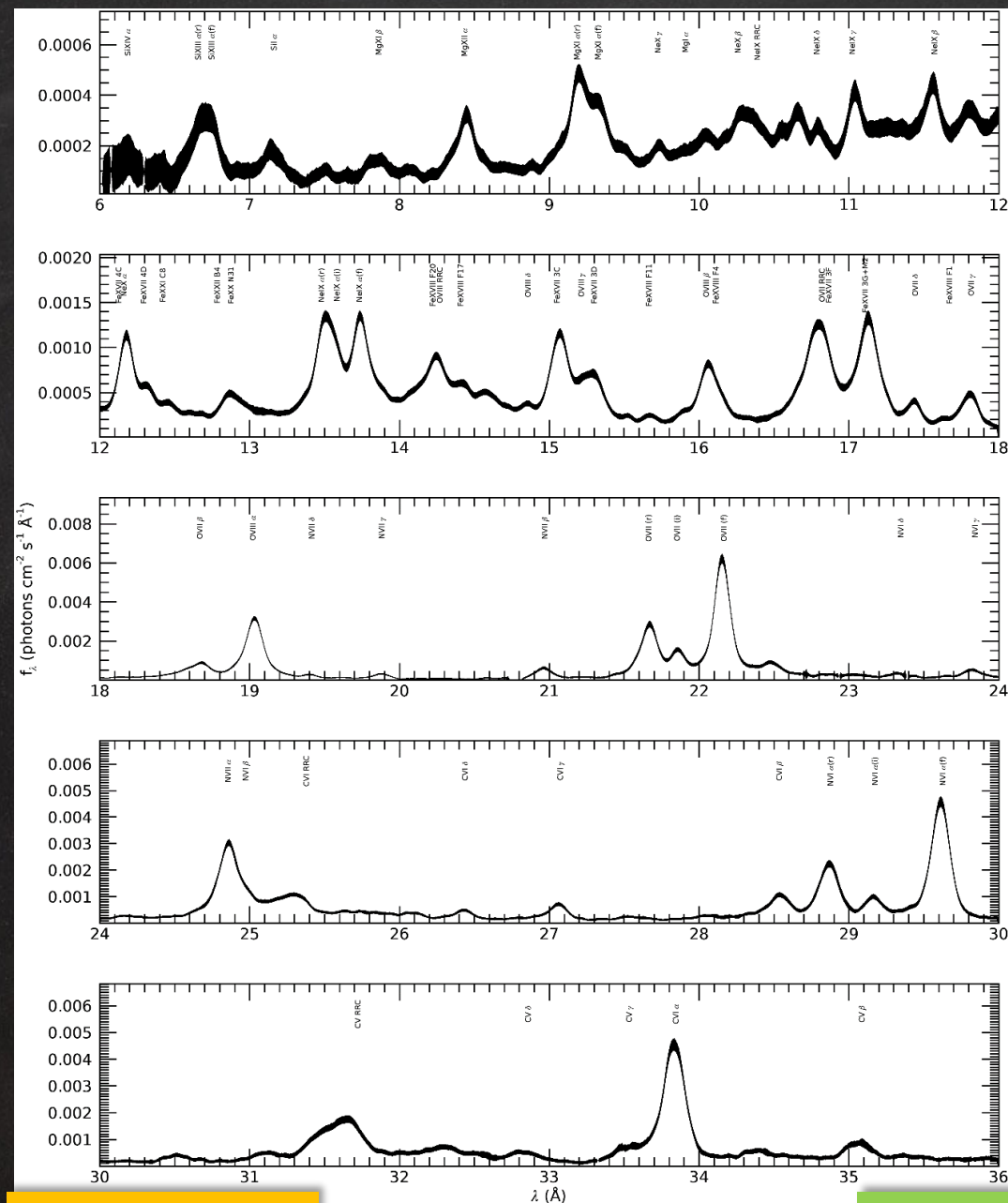
Dominated by **strong emission lines** with low or no continuum

Most of the 'soft excess' is concentrated in very strong lines easily detected even in very low SNR spectra

(e.g. Guainazzi & Bianchi, 2007)

Diagnostic ratios on triplets and higher order series lines point to **photoionization**, with an important role of photoexcitation

(e.g. Kinkhabwala+ 2002, Guainazzi & Bianchi, 2007)



THE EMISSION MEASURE DISTRIBUTION

EMISSION LINE LUMINOSITY

$$L = \int_V j_{ul}(\xi) dV$$

EMISSIVITY

$$j_{ul}(\xi)$$

IONIZATION PARAMETER


$$\xi = L_{ion}/n_e r^2$$

EMISSION MEASURE

$$EM = \int_V n_e^2 dV$$

LINE POWER

$$P_{ul}(\xi) = j_{ul}/n_e^2$$


$$L = \int_{\xi} d \log \xi \left[\frac{d(EM)}{d \log \xi} \right] P_{ul}(\xi)$$

The bracketed quantity above represents the **differential emission measure (DEM) distribution** (e.g. Liedahl 1999; Sako+ 1999)

In practice, the DEM distribution is the ensemble of weighting factors that determine the contributions of each ionization zone to the total line flux

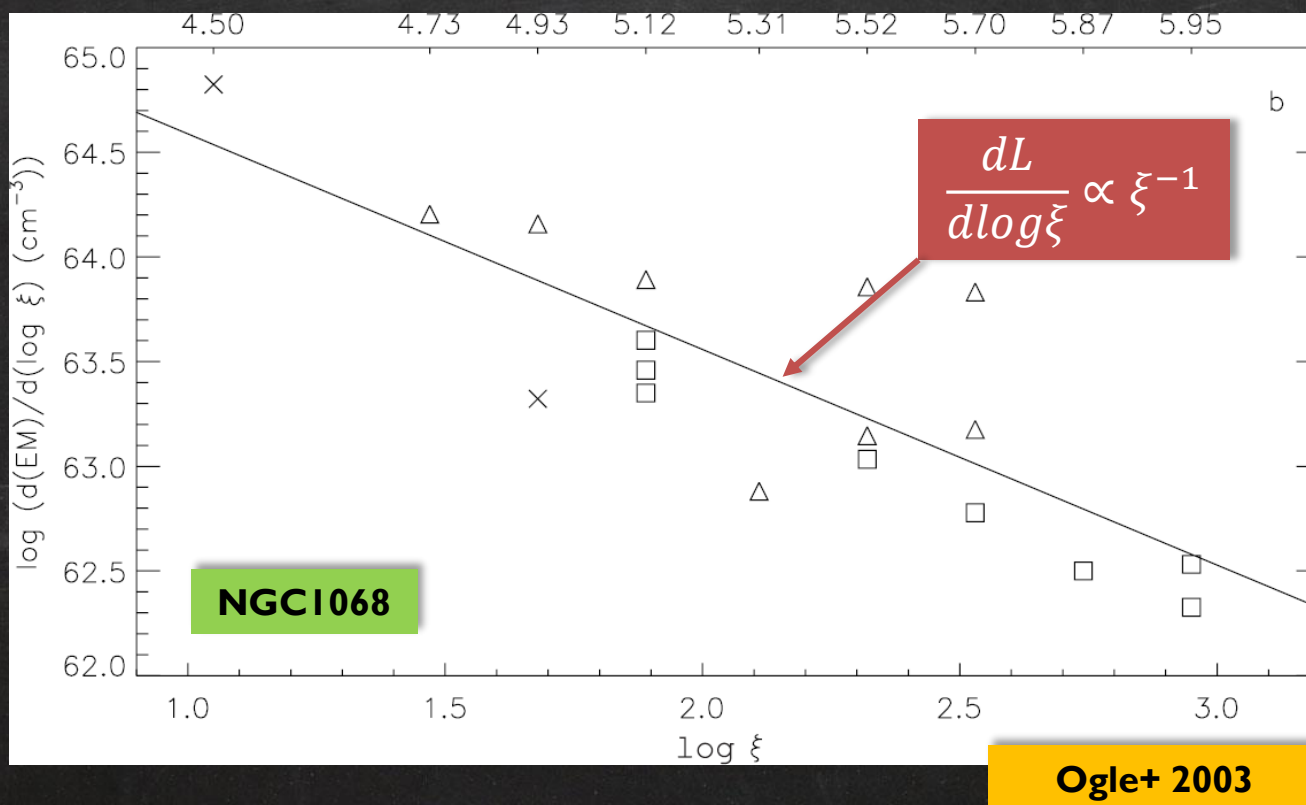
The usefulness of the DEM is that it can be derived theoretically for a given scenario, and readily compared to what is measured experimentally

CONSTANT DENSITY (LIEDAHL 1999)

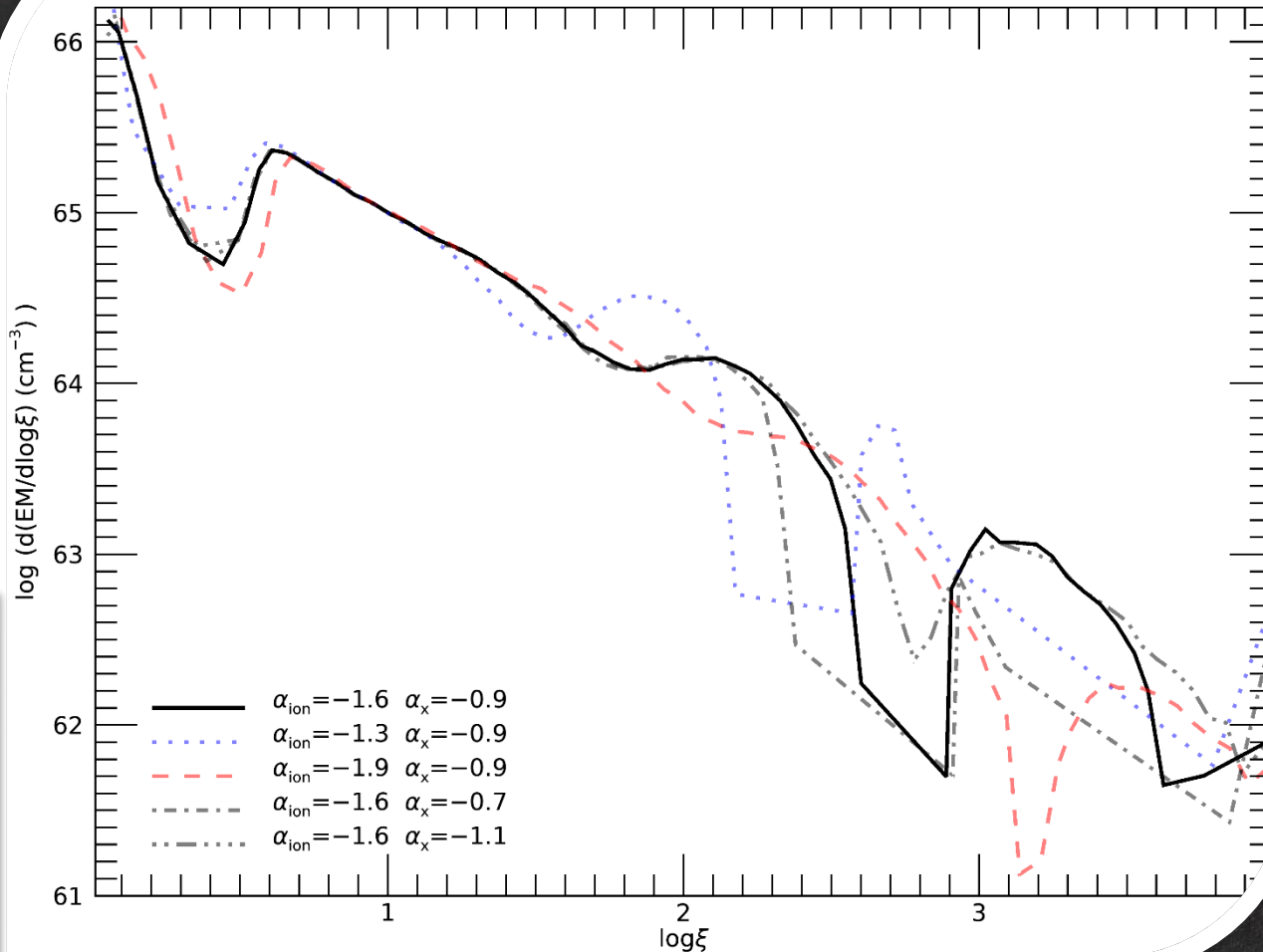
$$d(\text{EM}) / d \log \xi \propto \xi^{-3/2}$$

RPC (STERN+14, BIANCHI 2019A)

$$\frac{d}{d \log \xi} \text{EM} = 2.2 \cdot 10^{68} \Omega_{4\pi} L_{45} \xi^{-0.9} \text{cm}^{-3}$$



RPC: Differential Emission Measure Distribution

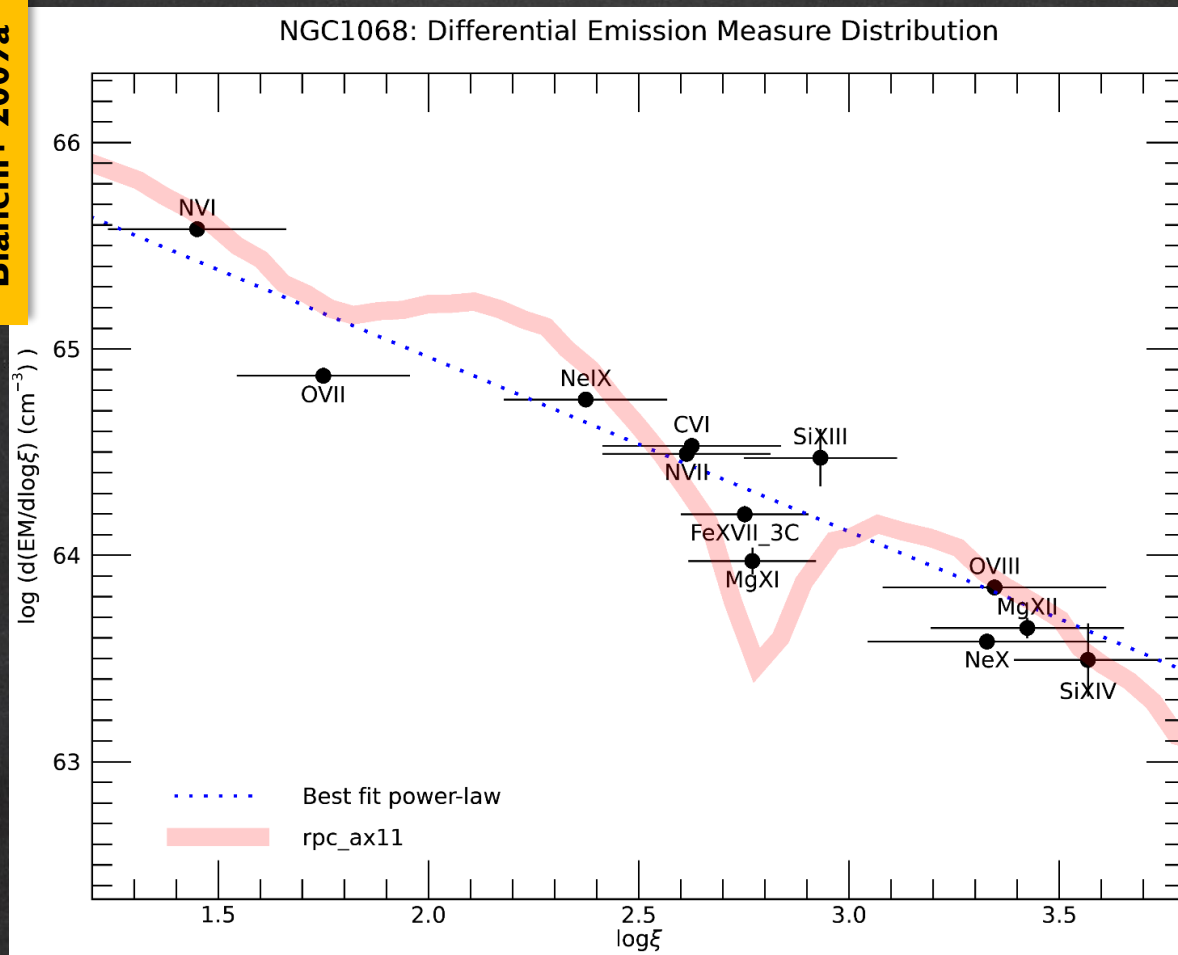


Bianchi+ 2019a

CLOUDY computations

The derived DEM in the case of RPC gas is very characteristic and robust against the specific gas parameters and illuminating SEDs

In practice, the DEM is basically set by the hydro-static equilibrium which the gas must obey in case of RPC, and does not depend on the other details

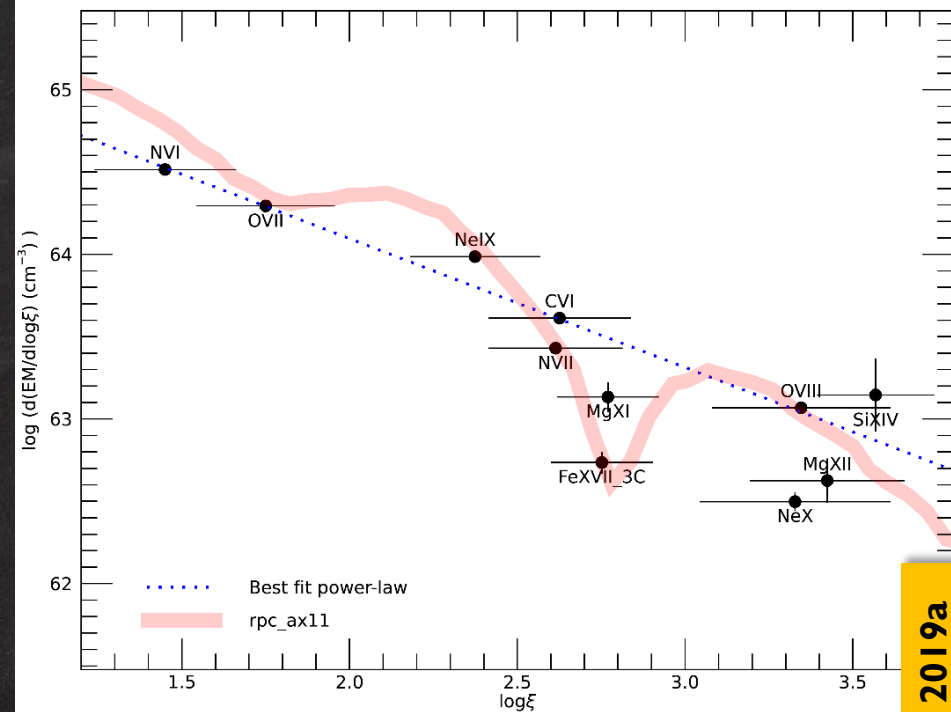


The observed DEM in NGC1068 evidently appears as a power-law distribution:
a linear regression gives a slope of ~ -0.85

The correspondence between the observed DEM and the distribution predicted for a RPC gas is impressive

It is important to stress that there are no free parameters in this comparison, apart from the average normalization of the two curves

NGC4151: Differential Emission Measure Distribution

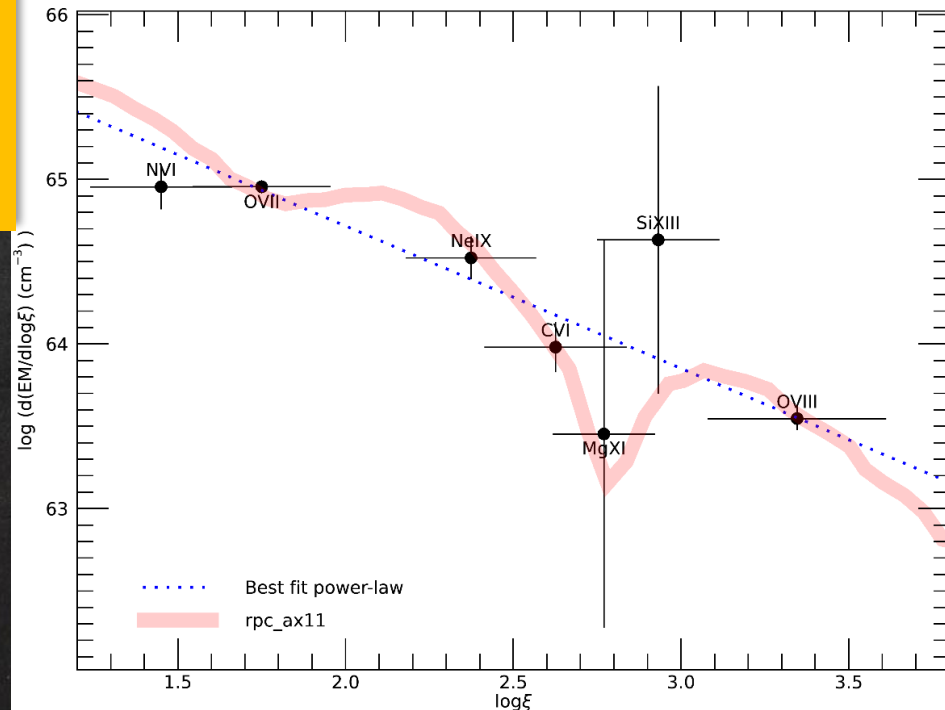


The observed DEM distribution of NGC 4151 is very similar to that of NGC 1068, again in extremely good agreement with the RPC predictions (slope ~ -0.78)

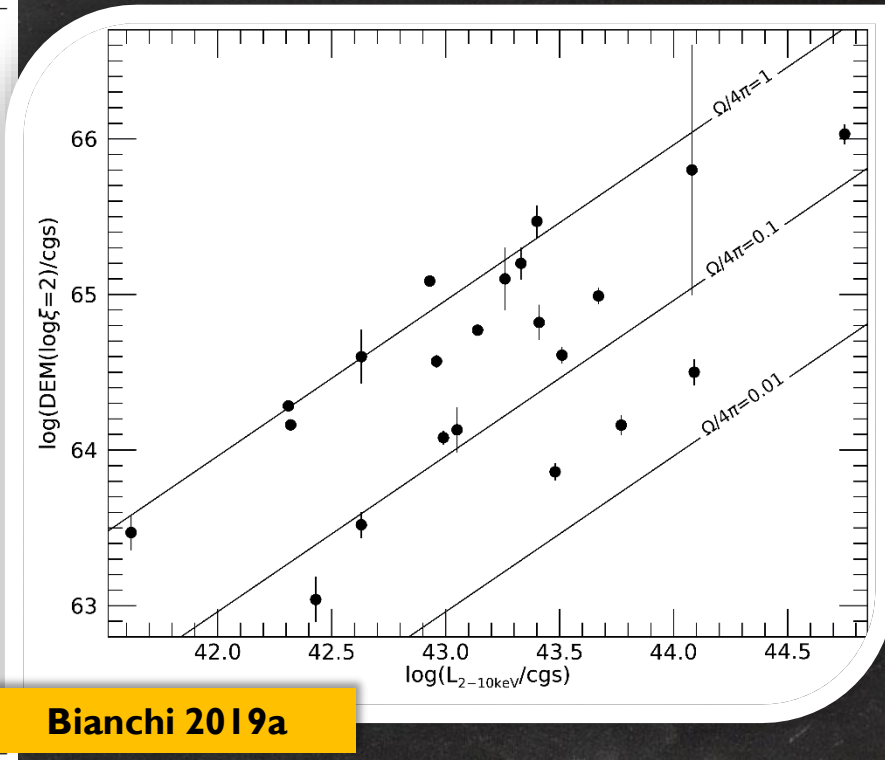
Bianchi+ 2019a

Very interesting case of NGC 5548: the archetypal Seyfert 1 is in an obscured state since (at least) 2012. Its soft X-ray emission is now the same as in Seyfert 2s (slope ~ -0.87)

NGC5548: Differential Emission Measure Distribution



Source (1)	$\log L_{2-10}$ (2)	Lines (3)	Best fit (4)	DEM ($\log \xi = 2$) (5)	DEM Slope (6)	$\Omega/4\pi$ (7)
NGC 1068	42.93	12	ax11	65.086 ± 0.004	-0.846 ± 0.006	1.567 ± 0.014
NGC 4151	42.31	11	ax11	64.284 ± 0.005	-0.782 ± 0.006	1.030 ± 0.012
NGC 1365	42.32	8	ax11	64.162 ± 0.019	-0.53 ± 0.04	0.76 ± 0.03
NGC 5548	43.14	7	ax11	64.77 ± 0.03	-0.87 ± 0.05	0.47 ± 0.03
Circinus	42.63	7	ax07	63.52 ± 0.08	-0.2 ± 0.2	$0.085^{+0.017}_{-0.014}$
NGC 7582	43.48	7	ax11	63.86 ± 0.05	-0.45 ± 0.09	0.026 ± 0.003
ESO362-G018	42.96	6	ax11	64.57 ± 0.04	-0.71 ± 0.06	0.45 ± 0.04
MRK 3	43.67	6	ax11	64.99 ± 0.05	-0.58 ± 0.07	$0.23^{+0.03}_{-0.02}$
NGC 4507	43.51	6	ax11	64.61 ± 0.05	-0.84 ± 0.08	$0.138^{+0.017}_{-0.013}$
NGC 5506	42.99	6	ax11	64.08 ± 0.04	-0.49 ± 0.09	$0.135^{+0.013}_{-0.012}$
IRAS05189-2524	43.40	5	ax11	65.47 ± 0.10	-0.6 ± 0.2	1.3 ± 0.3
NGC 424	43.77	5	aion16	64.16 ± 0.06	-0.91 ± 0.09	$0.027^{+0.004}_{-0.003}$
ESO138-G01	44.09	4	ax11	64.50 ± 0.08	-0.65 ± 0.12	$0.028^{+0.006}_{-0.005}$
MRK 477	43.26	4	ax11	65.1 ± 0.2	-0.9 ± 0.3	$0.8^{+0.4}_{-0.3}$
NGC 777	-	4	aion19	66.05 ± 0.04	-1.84 ± 0.13	-
NGC 1052	41.62	4	ax11	63.47 ± 0.11	-0.43 ± 0.19	$0.77^{+0.22}_{-0.17}$
NGC 5643	42.43	4	ax11	63.04 ± 0.14	-0.72 ± 0.18	$0.045^{+0.017}_{-0.012}$
NGC 6240	44.75	4	aion19	66.03 ± 0.06	-2.1 ± 0.2	0.21 ± 0.03
H0557-385	44.08	3	ax11	65.8 ± 0.8	0.30 ± 0.13	$0.6^{+3.0}_{-0.5}$
IRAS13197-1627	43.41	3	aion13	64.82 ± 0.11	-0.63 ± 0.18	$0.28^{+0.08}_{-0.06}$
MRK 231	-	3	ax07	65.46 ± 0.19	-0.2 ± 0.6	-
MRK 704	43.33	3	ax11	65.20 ± 0.10	-0.8 ± 0.3	$0.81^{+0.21}_{-0.17}$
NGC 1320	-	3	aion19	64.09 ± 0.17	-0.4 ± 0.4	-
NGC 3393	42.63	3	aion13	64.60 ± 0.17	-0.7 ± 0.2	$1.0^{+0.5}_{-0.3}$
NGC 4388	43.05	3	metals3	64.13 ± 0.14	-0.68 ± 0.18	$0.13^{+0.05}_{-0.04}$
UGC 1214	-	3	metals3	64.80 ± 0.16	-0.7 ± 0.2	-



No steeper DEMs than RPC:

- Lower N_H clouds can only flatten it (you must have the ionized layer!)
- No other gas compressing mechanism (i.e. magnetic), which can produce only dense photoionized gas

No apparent correlation between covering factor and luminosity

BLR line widths are driven by the BH gravity

KEPLERIAN MOTION

$$M_{\text{BH}}(H\beta) = \Delta v^2 R_{\text{BLR}} / G$$

$$M_{\text{BH}} = 10^{-21.7} \Delta v^2 L_{\text{bol}}^{1/2} M_{\odot}$$

$$\dot{m} = 10^{-16.4} \Delta v^{-2} L_{\text{bol}}^{1/2}$$

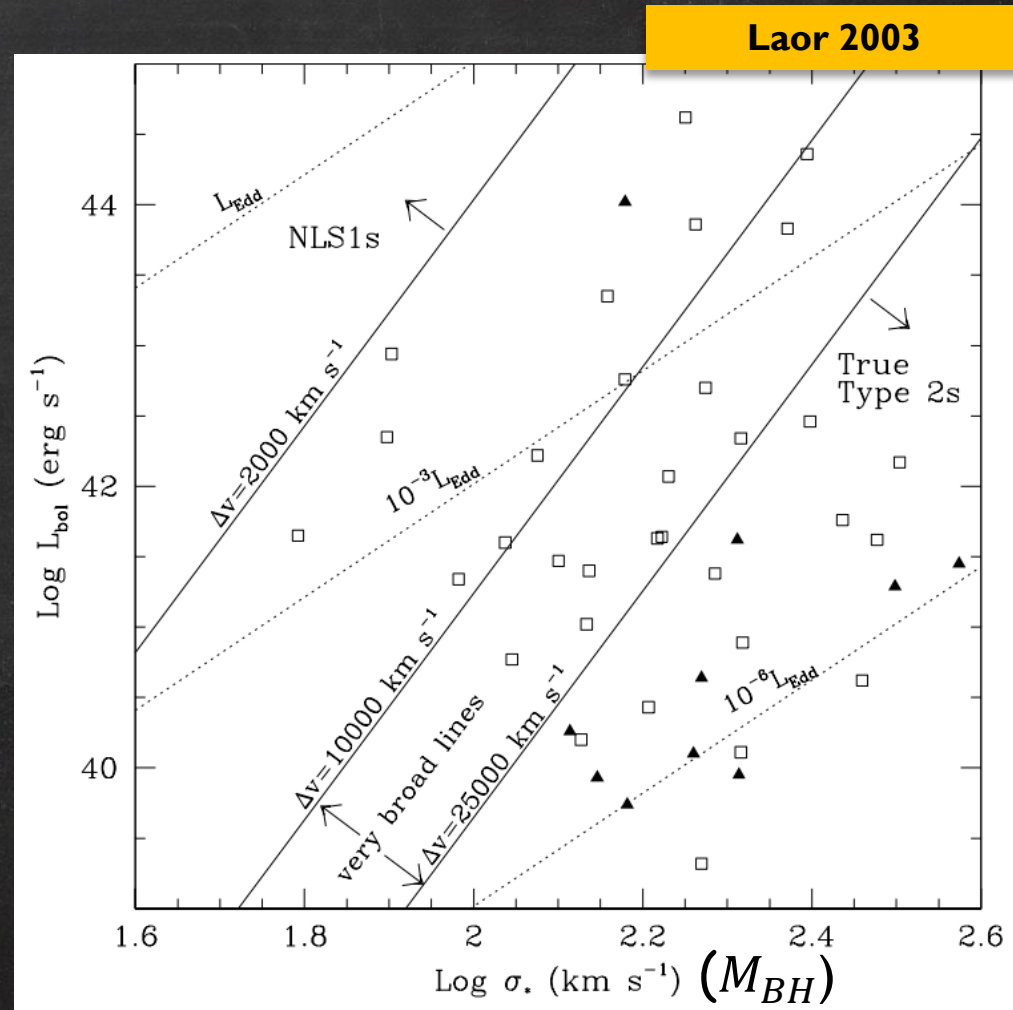
$$\Delta v = 21.1 M_{\text{BH}}^{1/4} \dot{m}^{-1/4}$$

$$\Delta v = 10^{10.85} M_{\text{BH}}^{1/2} L_{\text{bol}}^{-1/4}$$

Δv increases as M_{BH} increases and \dot{m} and L_{bol} decrease

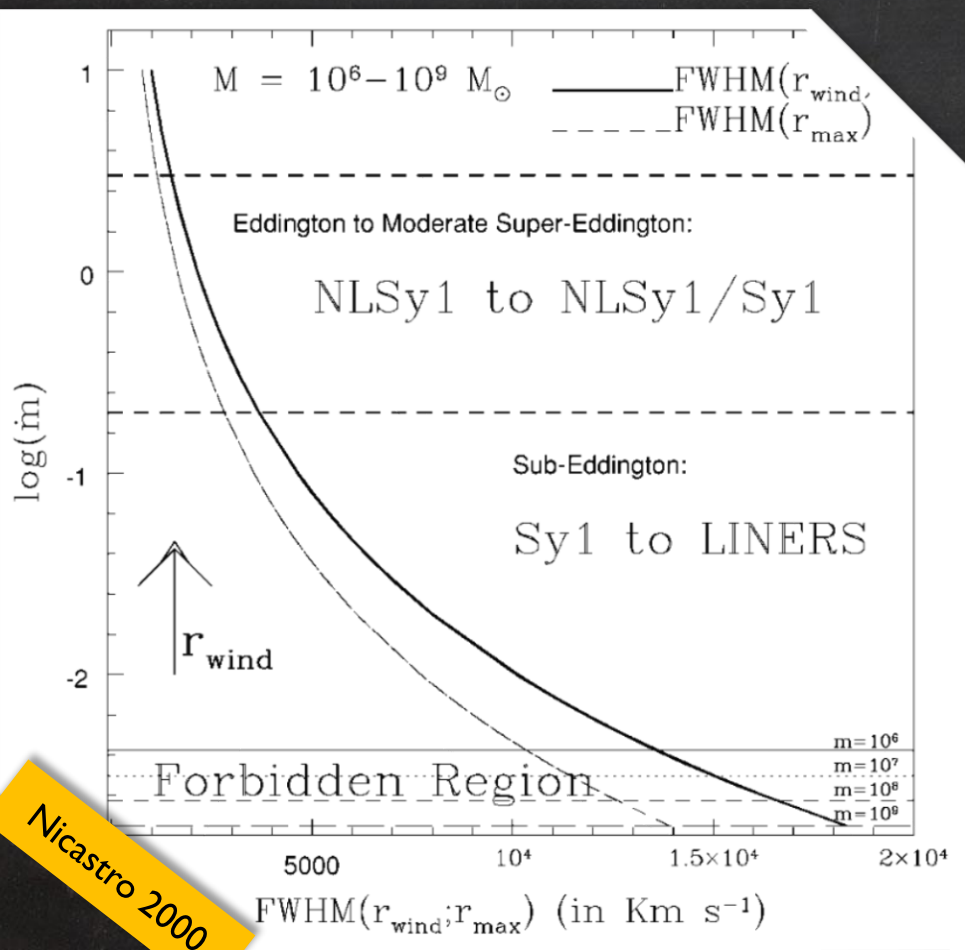
BLR RADIUS (DUST SUBLIMATION)

$$R_{\text{BLR}} = 0.086 (L_{\text{bol}} / 10^{46})^{1/2}$$



The lack of Balmer lines with $\Delta v > 25\,000\text{ km s}^{-1}$ may result from a physical upper limit on the velocity dispersion at which the BLR clouds can survive (Laor 2003)

No BLR is present when $L_{bol} < 10^{41.8} M_8^2$, or $\dot{m} < 10^{-4.3} M_8$



If the BLR is part of a disk wind, it cannot form if its launching radius falls below a critical radius: the innermost orbit of a classic Shakura & Sunyaev disk (Nicastro 2000), or the transition radius to a radiatively inefficient accretion flow (Trump+ 2011)

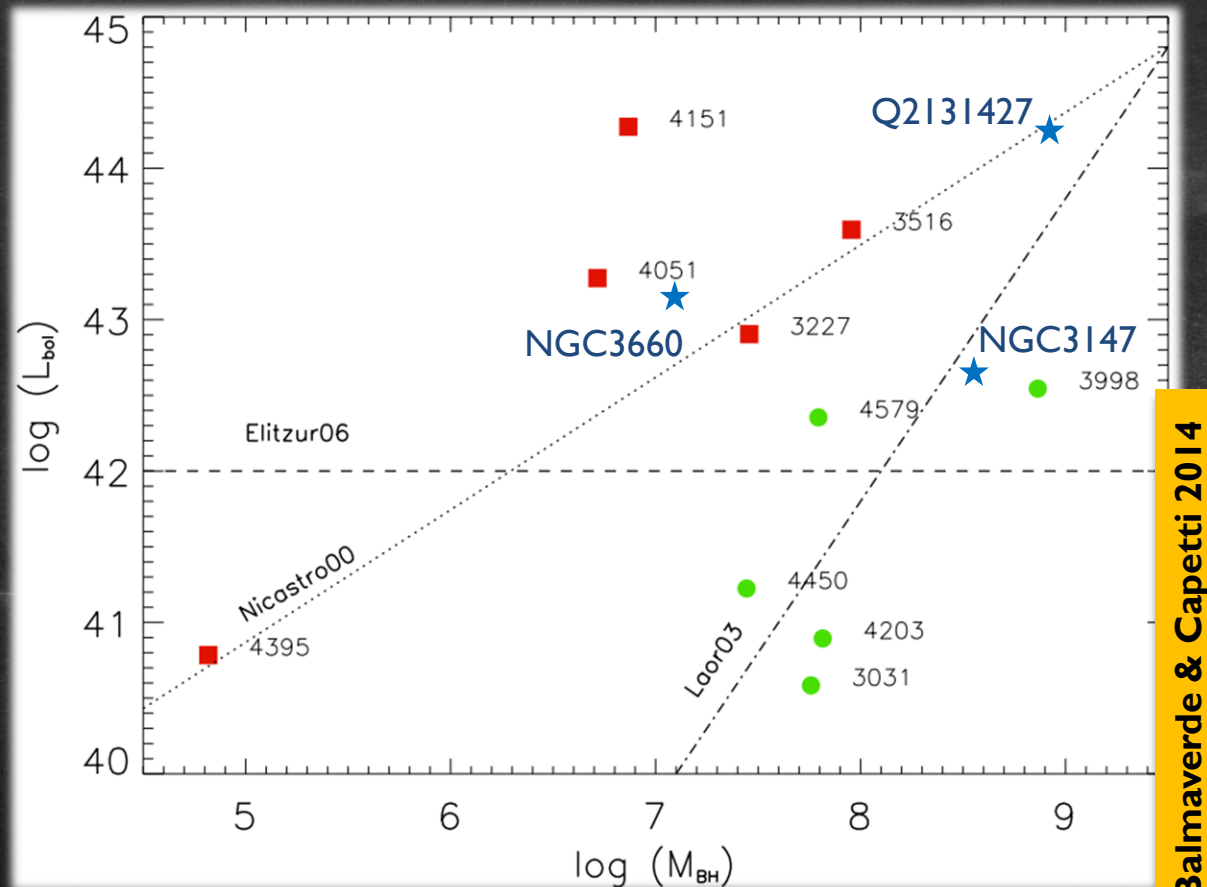
No BLR forms for Eddington rates lower than a critical value ($\sim 2 \times 10^{-3} M_8^{-1/8}$)

Nicastro 2000

If the BLR cannot form in weakly accreting AGN, we expect the existence of “true” Seyfert 2 galaxies: optically Type 2 objects, without obscuration

The best candidates are found with simultaneous optical/X-ray observations:

NGC3147 ($4 \times 10^{-5} - 3 \times 10^{-4}$: Bianchi+2008, 2017), **Q2131427** ($2 - 3 \times 10^{-3}$: Panessa+ 2009), **NGC3660** ($4 \times 10^{-3} - 2 \times 10^{-2}$: Bianchi+, 2012)



Have the above theoretical predictions, that the BLR disappears at very low luminosities/accretion rates, indeed been vindicated by these objects?

Be careful:

- low L_{bol}/L_{Edd} AGN are heavily dominated by the host galaxy emission
- low L_{bol} – high M_{BH} make the lines extremely broad, even harder to detect

NGC3147: THE BEST CANDIDATE

$$3.1 \times 10^8 M_{\odot}$$

$$4 \times 10^{42} \text{ erg s}^{-1}$$

$$\text{FWHM}_{\text{H}\alpha} \simeq 7088 \left(\frac{M_{BH}}{10^8 M_{\odot}} \right)^{0.49} \left(\frac{L_{bol}}{10^{44}} \right)^{-0.26} \text{ km s}^{-1}$$

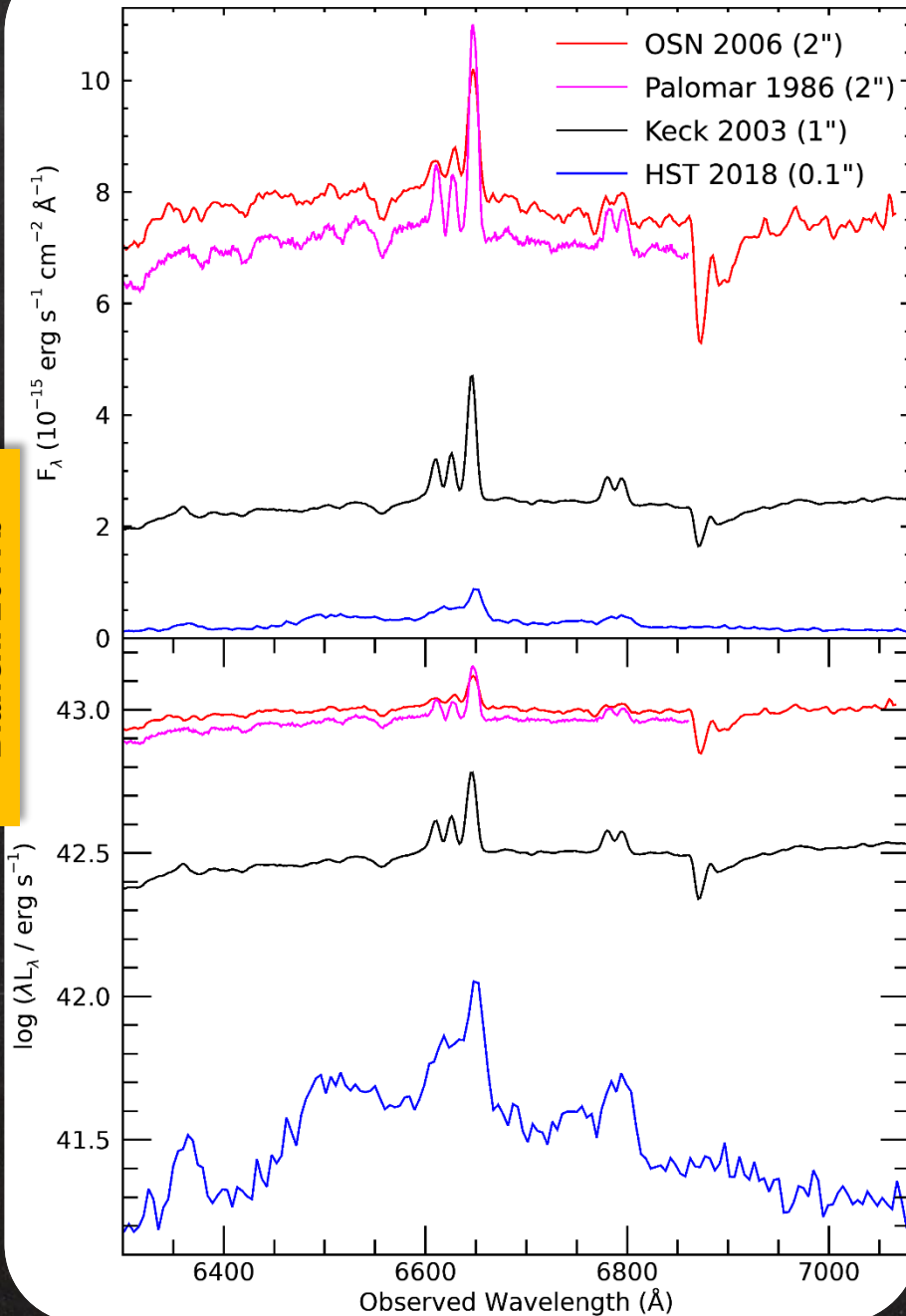
Stern&Laor 2012,
Bianchi+2012

$$\text{FWHM}_{\text{H}\alpha} \simeq 28\,000 \text{ km s}^{-1}$$

The only way to definitely exclude the predicted BLR emission is HST spectroscopy

The HST narrow slit (0.1") can exclude the bulk of the host emission, and reveal if the expected very broad H α is indeed present

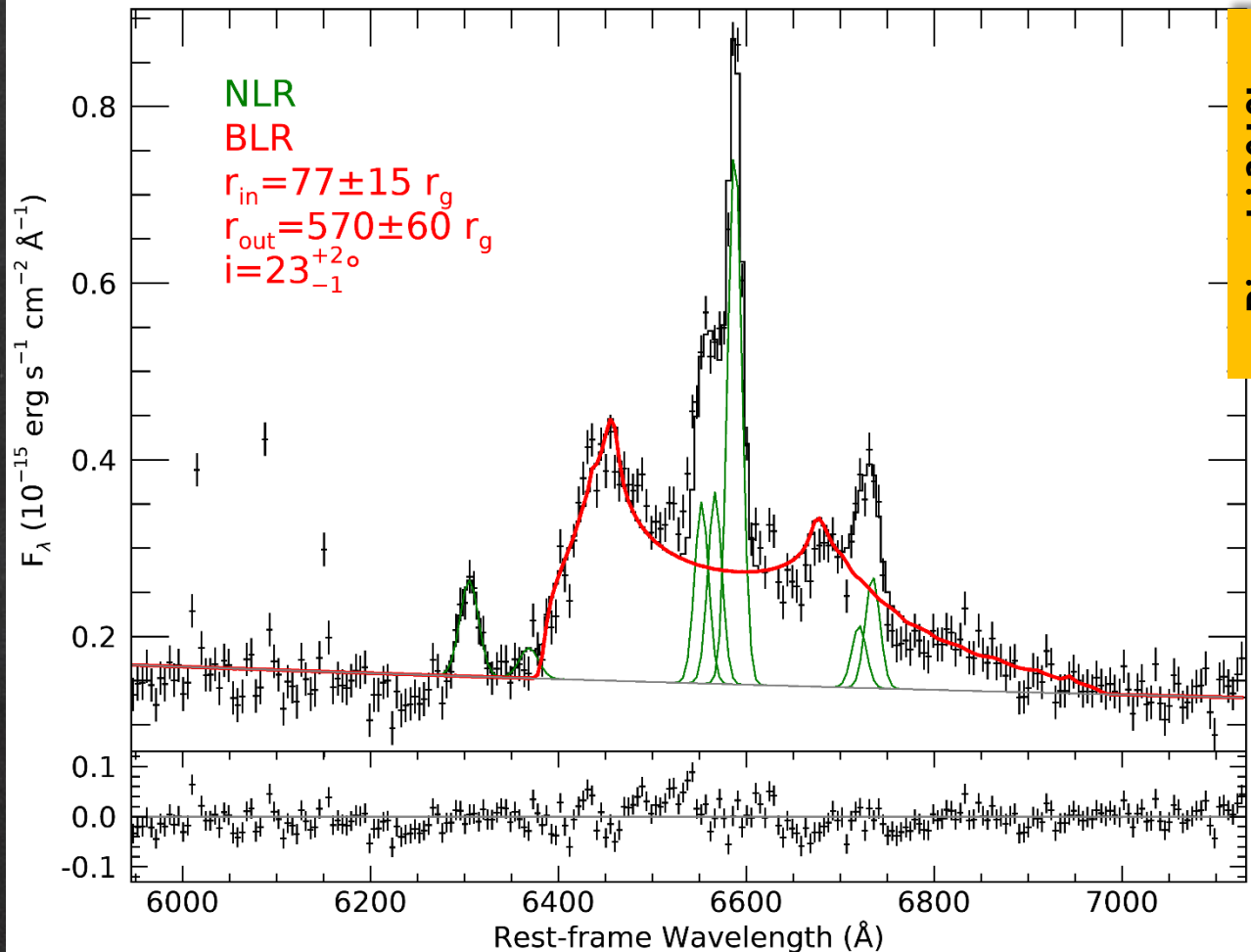
NGC3147



The small slit width hugely reduces the host contamination

An H α line with an extremely broad base (FWZI $\sim 27\,000 \text{ km s}^{-1}$) is now evident!

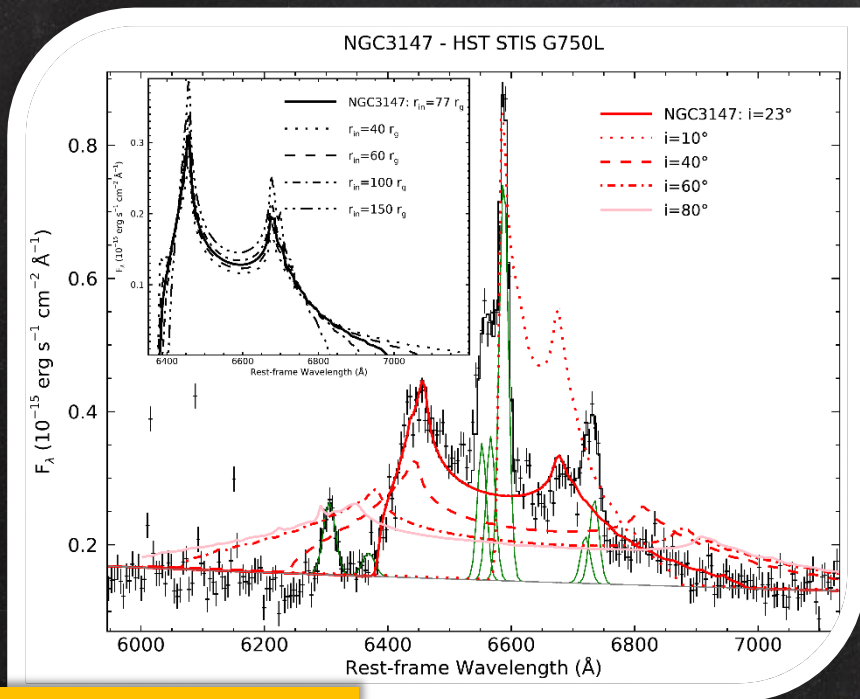
NGC 3147 is not a true type 2 AGN



The line profile shows a steep cutoff blue wing and an extended red wing, which match the signature of a **mildly relativistic thin accretion disk line profile**

It is indeed well fit with a nearly face on thin disk with an inner radius at $77 \pm 15 r_g$, which matches the prediction of $62_{-14}^{+18} r_g$ from the $R_{\text{BLR}} \sim L^{1/2}$ relation

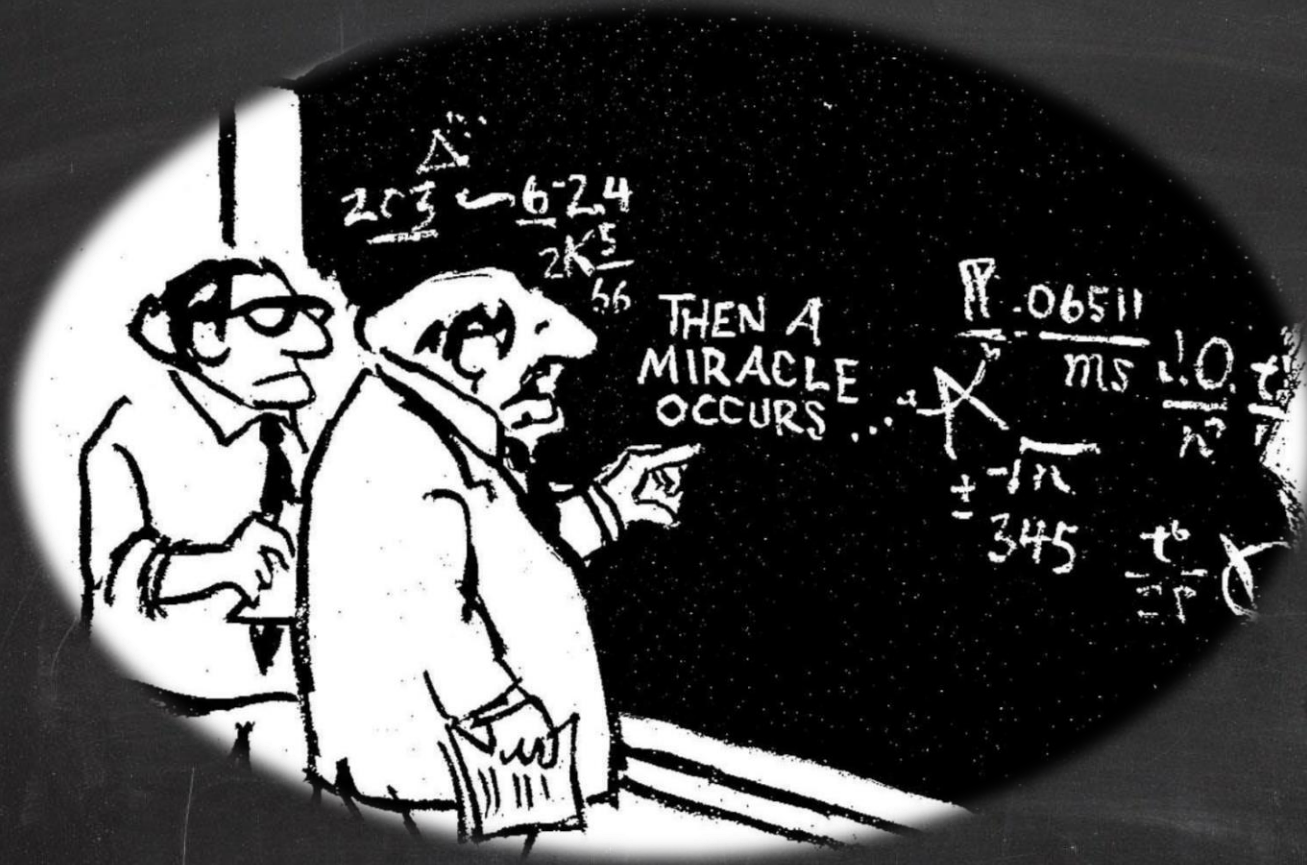
The luminosity of the broad H α line is consistent with the predicted values from the X-ray and [O III] luminosities (Stern & Laor2012a,b): NGC 3147 appears like a standard type I AGN at the very low end of luminosity ranges



Bianchi 2019b

H α disk line profiles have been observed in a handful of objects: here we find that the BLR forms a thin disk, extending down well below $100 r_g$. A thin accretion disk at $L/L_{\text{Edd}} \sim 10^{-4}$ is in contradiction with the standard paradigm, that at low accretion rates, the accretion configuration becomes optically thin and quasi-spherical (Blandford & Begelman 1999)

Optical detections of relativistic line profiles may provide a new tool to explore the innermost disk structure



“You put a cloud of gas at some distance from the AGN, and the rest is set by nature.”

(Ari Laor)

BASIC REFERENCES

Bianchi, Guainazzi, Laor, Stern, Behar, 2019a, MNRAS, 485, 1

Bianchi, Antonucci, Capetti, Chiaberge, Laor, et al., 2019b, MNRAS in press